Supplementary Information for

Experimental Evidence for a Charge-Transfer Intermediate in Pentacene Singlet Fission

Stephanie M. Hart, W. Ruchira Silva, Renee R. Frontiera*

Department of Chemistry, University of Minnesota, 207 Pleasant St SE, Minneapolis, MN

*To whom correspondence should be addressed. rrf@umn.edu, 612.624.2501

Contents

1. Actinic Pump Spectrum

The spectrum of the actinic pump is shown in Figure S1. The pulse had a central wavelength of 573 nm with full width at half maximum value of 17 nm.

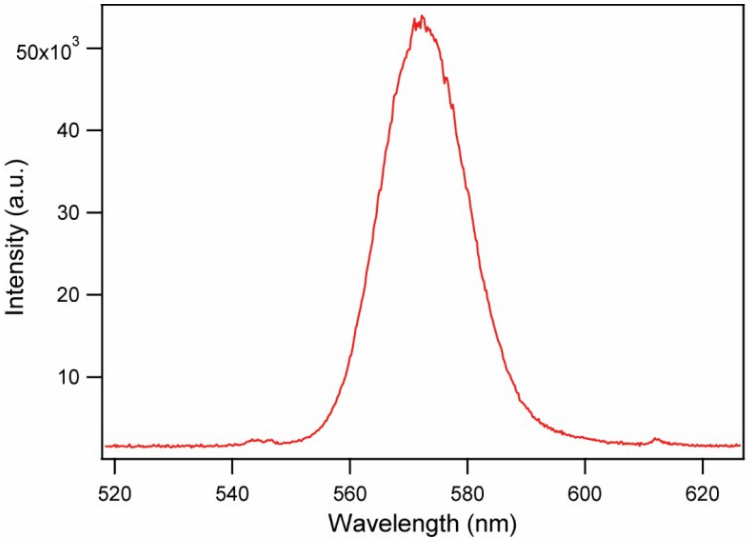

Figure S1: Actinic pump spectral profile.

2. Ground State Addition Process

The FSRS data after one-to-one subtraction of the ground state and before any ground state addition are shown in Figure 2a of the main text. As discussed, the ground state addition used in the data analysis consisted of adding ground state spectra back into the spectra seen in Figure 2a until no negative features at ground state frequencies remained. However, this criterion is somewhat subjective, and here we explore another method of the ground state addition process. Figure S2 shows the FSRS spectra in which the ground state was added back in at an amplitude such that no spectral splitting features remain. This figure can be directly compared to the spectra shown in Figure 2b of the main text.

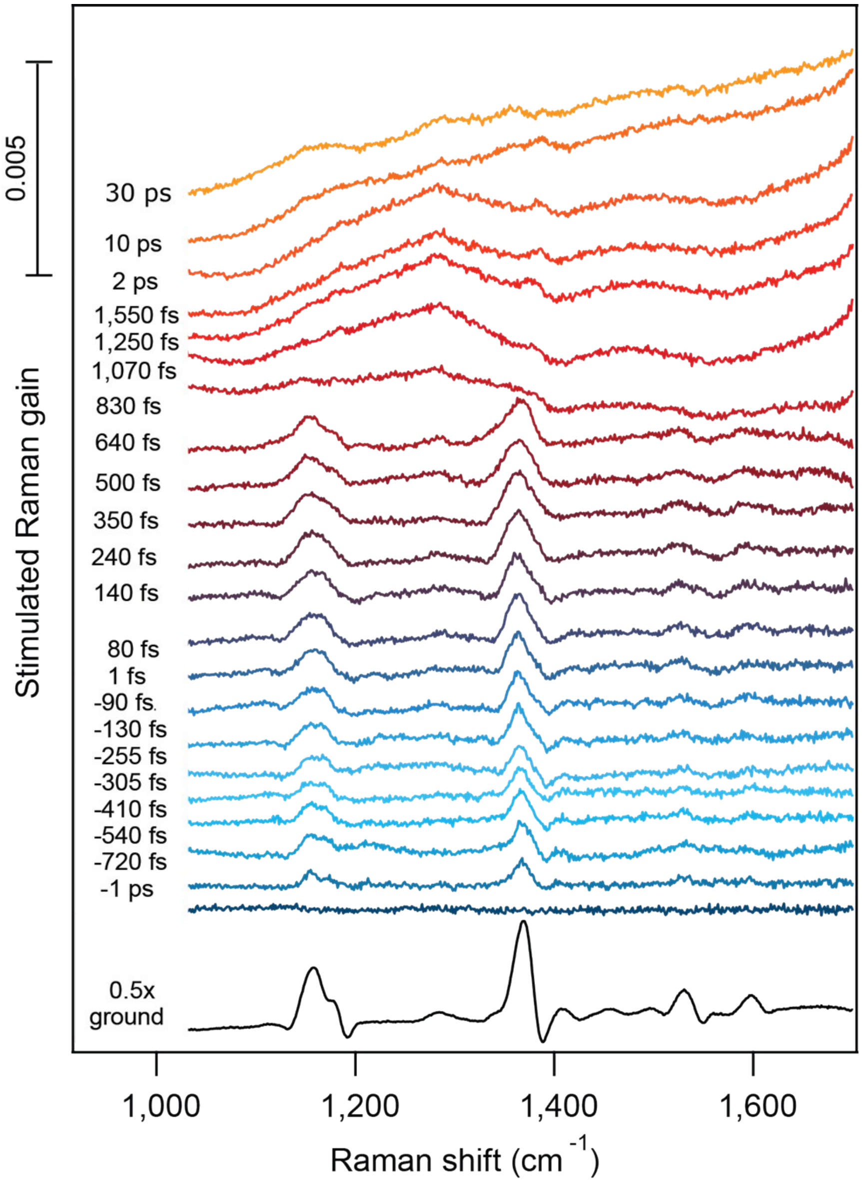

Figure S2: Differential stimulated Raman spectra after alternate ground state addition procedure.

With this alternate ground state addition procedure, the FSRS data are characterized by an intermediate state with significantly broadened features at ground state frequencies. Several physical phenomena could give rise to these broad features. One plausible explanation includes the presence of a conical intersection in the reaction pathway from the singlet to the triplet state, which could potentially truncate the FSRS vibrational coherence, leading to peak broadening as the wavepacket approaches the intersection. However, work by two independent studies proves that vibrational coherences created on the initially prepared excited state in pentacene survive passage through a conical intersection.[1-2] This suggests that any conical intersections on the singlet fission reaction pathway are unlikely to truncate the FSRS vibrational coherence. Thus, we cannot attribute the short-lived broad spectral features seen in in Figure S2 to vibrational coherence truncation by a conical intersection.

A second physical phenomenon that could give rise to broad features immediately after photoexcitation could be exciton delocalization on the ultrafast timescale. The charge transfer states associated with pentacene are highly delocalized in nature, and thus in the FSRS measurements we could be sampling a larger number of molecules at very early time points and therefore could probe more defects in the pentacene crystals, thus yielding more extensive heterogeneous broadening at very early time points.[3] This could cause peak broadening on a ~100 fs timescale before subsequent exciton localization causing the peaks to become less broad at later times. The peak width, as measured by the full-width at half maximum (FWHM), increases as a function of time throughout the 1 ps time interval. If exciton delocalization were to give rise to the broad spectral features seen in Figure S2, we would expect to see the peak width increase for 100 fs before subsequently decreasing at later time points. Conversely, the observed continual increase in peak width as a function of nominal time delay suggests that exciton delocalization could not feasibly give rise to the broad peaks seen in Figure S2.

A further point to consider in examining figure S2 are the peak lineshapes. In the FSR spectra we typically expect the peaks to have Gaussian lineshapes, as inhomogeneous broadening and convolution with the instrument response function dominates compared lifetime broadening. However, the largest peak in the Figure S2 spectra, the 1363 cm^{-1} peak, has a skew normal distribution lineshape. Furthermore, the direction of skew changes transiently from a positive to a negative skew shape parameter over the -720 fs to +640 fs time interval. It is challenging to assign a physical phenomenon that could give rise to a transient shift in the skew normal distribution other than the presence of two peaks with changing magnitudes forming the single broad peak detected at 1363 cm^{-1}.

We are not able to assign a physical phenomenon that could give rise to features seen in Figure S2. As such, this lack of physical explanation for the spectra in Figure S2 leads us to use the ground state addition technique giving rise to the spectra seen in the main text Figure 2b. Further comparison of the two can be seen in Figure S3 showing the ground state depletion kinetics of the main text Figure 2b and Figure S2. Here the cross-correlation (FWHM 410 ± 10 fs) is shown along with the amount of ground state added back into each set of spectra to give rise to the features seen in Figures 2b and S2. Use of the alternate ground state addition procedure (giving rise to Figure S2) leads to the appearance of transient features at unrealistically early timescales.

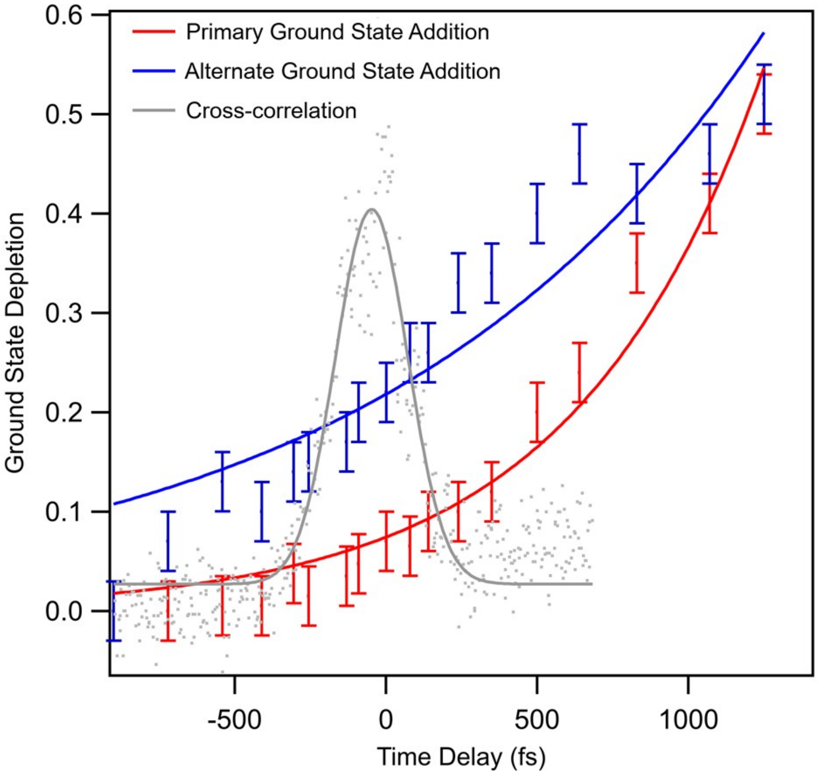

Figure S3: Ground state depletion kinetics accounted for in the primary ground state addition (seen in main text Figure 2b) and the alternate ground state addition (Supplemental, Figure S2) along with cross-correlation trace. Exponential fits to the experimental data are shown.

3. Peak Fitting Procedure

All excited state peaks were fit to a Gaussian profile with a third order polynomial background to account for the electronic transient absorption, as shown in Figure S4 below.

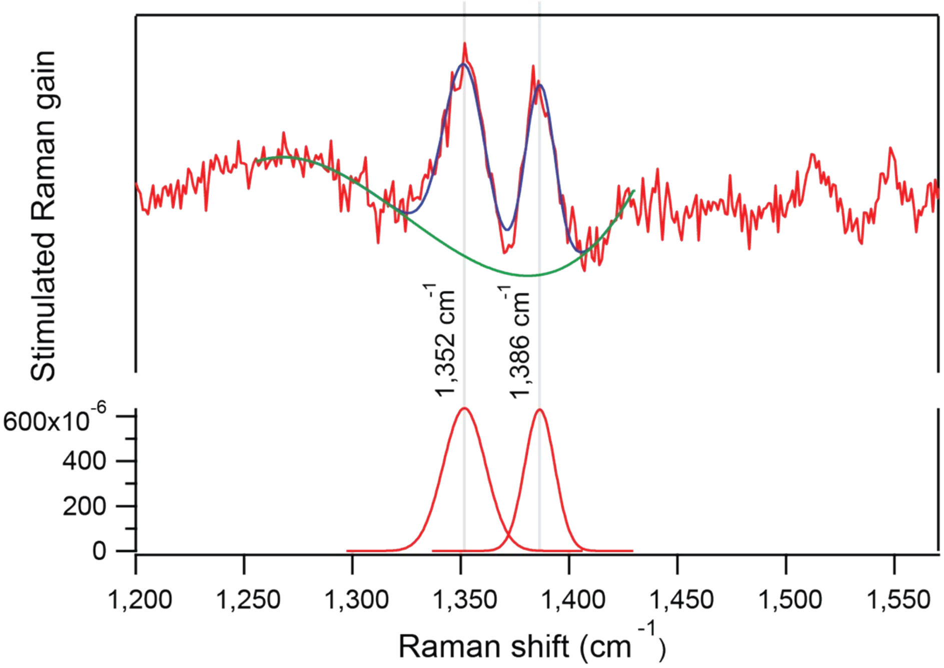

Figure S4: Femtosecond stimulated Raman spectra at a time delay of 500 fs after photoexcitation. The top plot shows the experimental data along with the fits (in blue) and the third order polynomial baseline (in green). The bottom plot shows the Gaussian fits of the two peaks at 1352 cm^{-1} and 1386 cm^{-1}.

4. Pentacene Transient Absorption

As discussed in the main text, a change in resonance conditions upon formation of the triplet state in pentacene results in photoinduced absorption from 750-950 nm. This is seen in the transient absorption plot in Figure S5, which has been corrected for chirp.[4] The transient absorption feature persists for tens of picoseconds, the timescale over which the long-lived triplet state in pentacene is expected to exist. The kinetics and further discussion of the transient absorption feature relative to the charge-transfer state dynamics is presented in the main text.

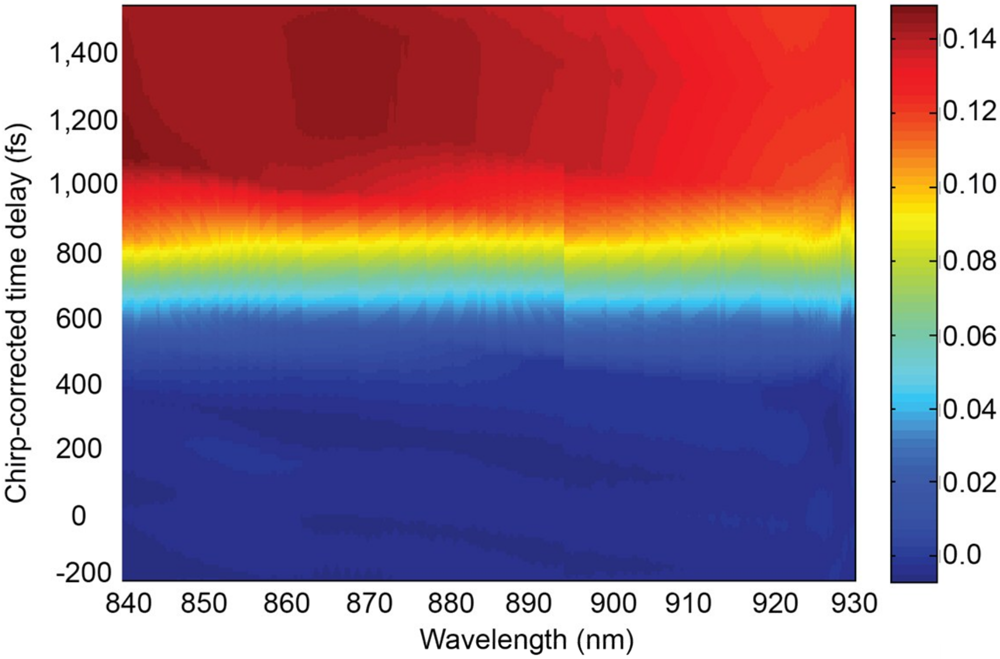

Figure S5: Pentacene transient absorption traces at chirp-corrected time delays after photoexcitation. The transient absorption beginning near time zero arises due to a change in the resonance conditions upon formation of the triplet state. This feature persists for tens of picoseconds after photoexcitation.

5. Actinic Pump Power Dependence Study

An actinic pump power dependence study was performed in order to ensure that measurements were taken in the linear regime. The same sample was used in four FSRS experiments of varying average actinic pump power from 3-14 uW. The FSRS spectra at nominal time delays for four powers, 14 uW, 8 uW, 5 uW, and 3 uW, are shown in Figure S6. As seen in panel D, a 3 uW actinic pump power was not sufficient to resolve any transient features. Powers examined above 14 uW resulted in sample degradation as evidenced by loss of ground state Raman signal. The cross correlation for these power dependence experiments was 530 ± 20 fs as measured by the optical Kerr effect in cyclohexane. Due to differences in the thickness of the cyclohexane sample with the pentacene sample leading to variations in time zero, the time delays in figures S6-S10 were offset such that the transient absorption kinetics were in agreement with the data presented in the main text.

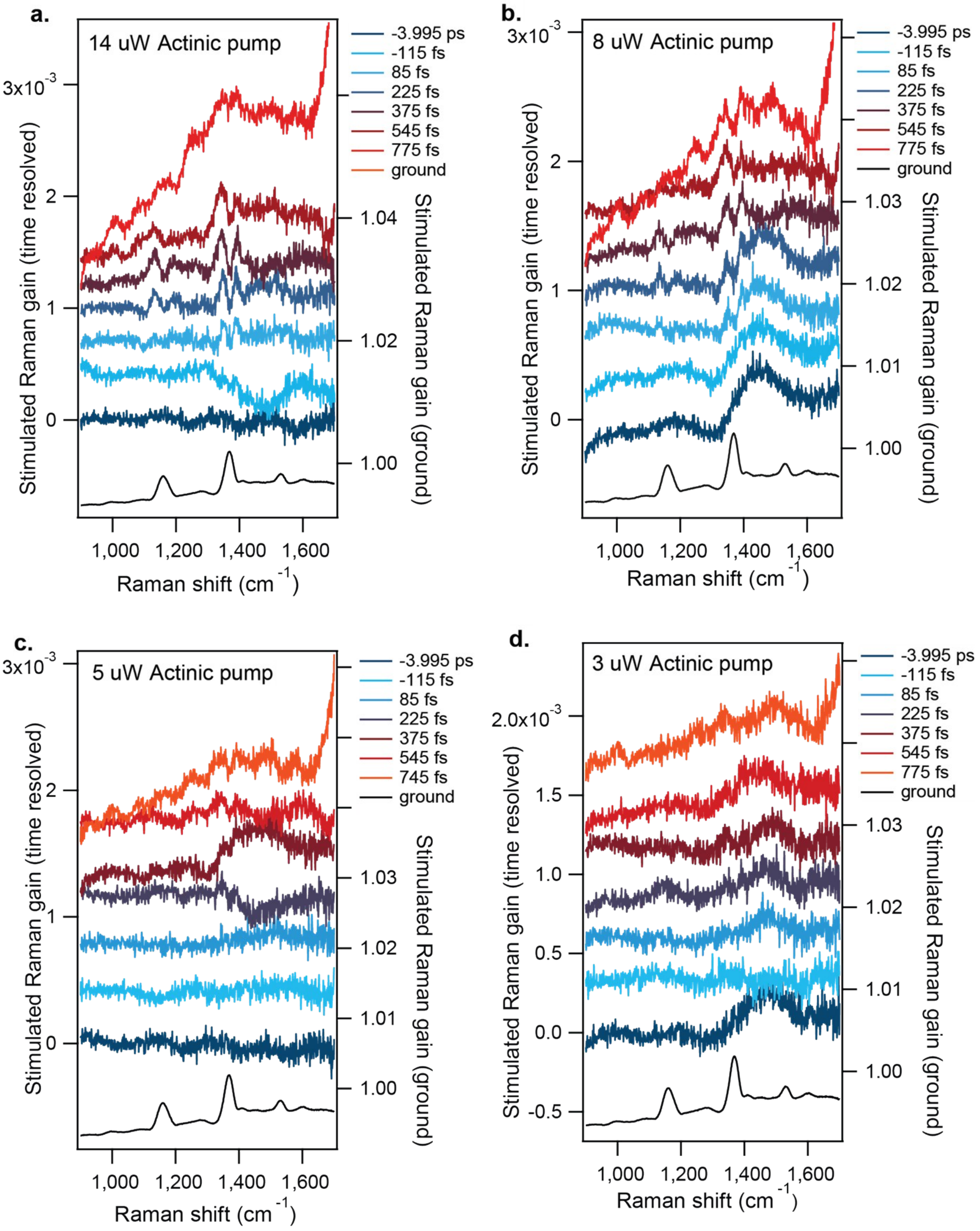

Figure S6: FSR spectra at time delays after photoexcitation for varying actinic pump powers of a. 14 uW, b. 8 uW, c. 5 uW, and d. 3 uW.

Figure S7 shows the actinic pump power dependence for two different peaks at two time points. Within the range of accessible actinic pump values, the features are linear, with linear fits giving r^2 values between 0.921 and 0.988. Given the linear dependence, we can safely assume that photoexcited pentacene molecules were sufficiently spatially separated such that these molecules were not interacting with other photoexcited molecules undergoing singlet fission.

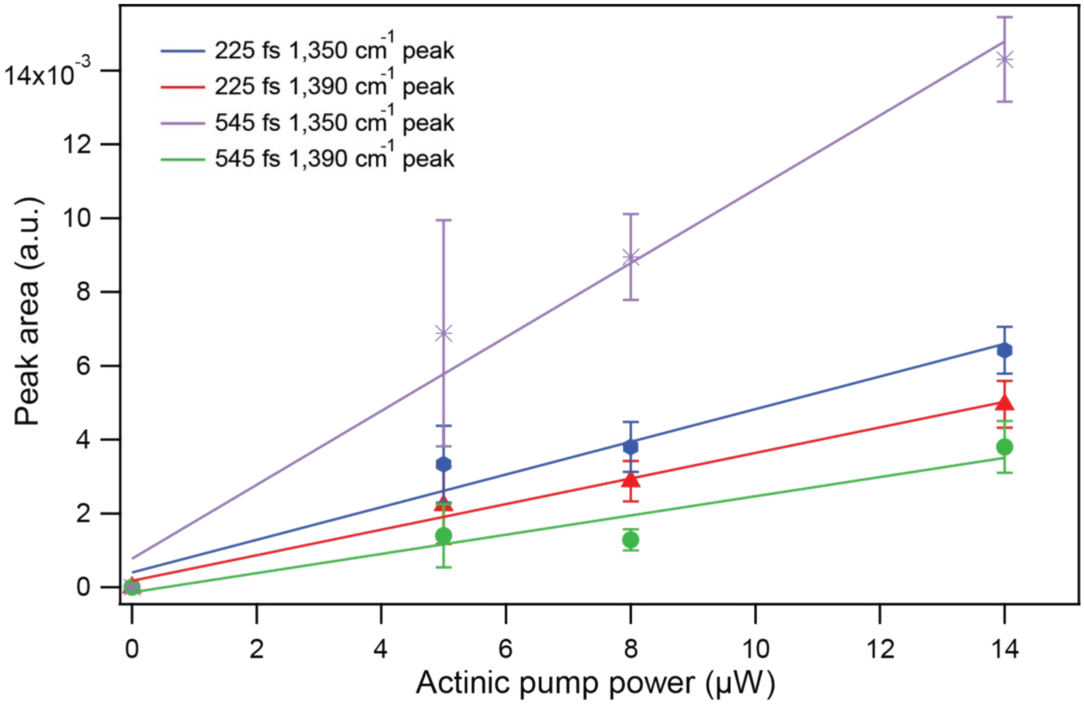

Figure S7: 1350 cm^{-1} and 1390 cm^{-1} peak area as function of actinic pump power at time delays of 225 fs and 545 fs.

Figure S9 shows the maximum magnitude of the 840 nm triplet excited state absorption as a function of actinic pump power corresponding to the Raman measurements in Figure S8. Over the power range examined the magnitude of excited state absorption appears to be linear with excitation power given the linear $R^2=0.98$ trend line shown. The exponential rise times (not convolved with the instrument response) are given in Table S1 for each power examined, ranging from 230-240 fs. Thus, within error the transient absorption feature kinetics do not vary as a function of excitation power. Given the linearity in power dependence and identical kinetics at varying excitation power, we are likely in the low excitation density regime as to avoid triplet annihilation events.

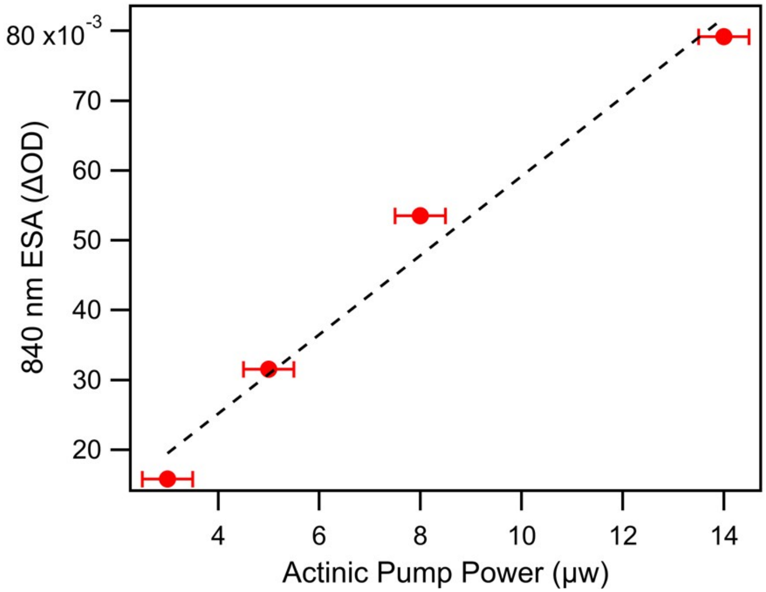

Figure S8: Maximum intensity of 840 nm excited state absorption feature as a function of excitation power.

6. Raman Pump Power Dependence Study

A Raman pump power dependence study was conducted to verify that FSRS signals were acquired in the linear regime. These experiments were conducted with a lens in place of the 20x microscope objective to focus all three FSRS pulses to the sample. As such, greater powers were used for the actinic pump and the Raman pump in order to achieve the same flux with a larger beam spot size. The cross correlation for these power dependence experiments was 240 ± 15 fs as measured by the optical Kerr effect in diamond. The actinic pump power was 420 μW, and the transient absorption kinetics showed no changes with changing Raman pump power. Average powers with values between 0.17 and 0.385 mW were used. The transient Raman features as a function of Raman pump power are shown in Figure S9. The linear fits shown have r^2 values ranging from 0.874-0.889. With these data we therefore we do not see any strong indications that the excited state peak areas exhibit a non-linear Raman pump power dependence.

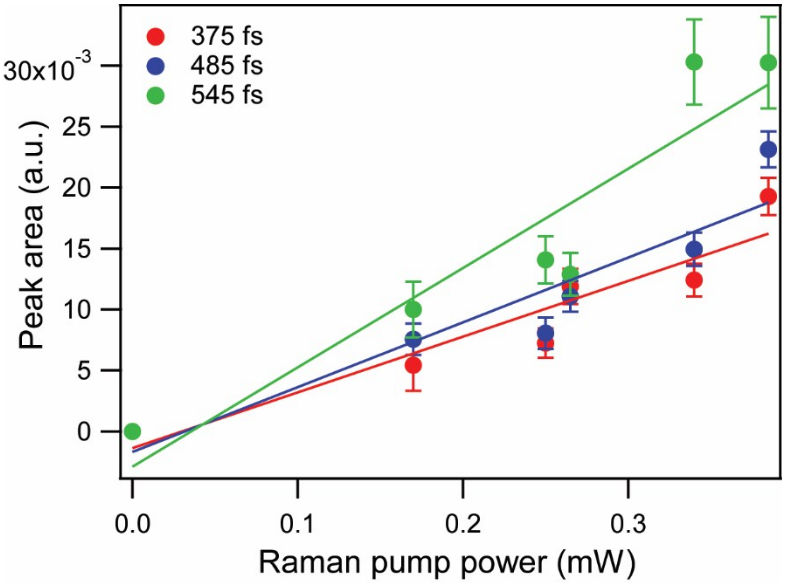

Figure S9: Raman pump power dependence with linear fits for the 1400 cm^{-1} excited state peak at time delays of 375 fs, 485 fs, and 545 fs.

7. Etalon Raman Pump Experiment

The Raman pump used for all data shown in the main text was generated through a grating filter, thus creating a pulse with a 2.1 ps Gaussian temporal profile. In order to verify that excess Raman pump photons hitting the sample before time zero were not leading to any experimental artifacts in the data, we replicated our FSRS experiments but replaced the grating filter with a Fabry-Perot etalon, which provides an exponential temporal profile.[5] In these experiments a lens was used in place of the 20x microscope objective. Here the cross-correlation time was 130 fs ± 7 fs as measured by the optical Kerr effect in diamond.

Figure S10 shows the differential stimulated Raman spectra at time points relative to photoexcitation with use of the Fabry-Perot etalon. As seen in this figure, spectral splitting of the ground state peaks occurs when the molecules are promoted to the excited state, indicative of a charge-transfer intermediate as was discussed in the main text.

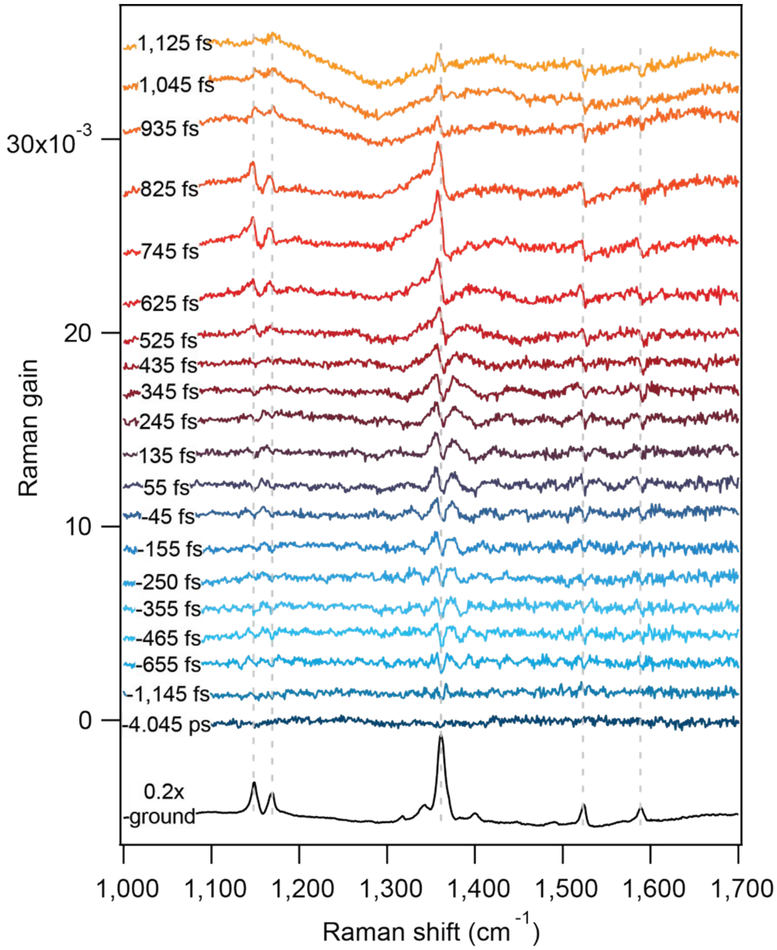

Figure S10: Differential stimulated Raman spectra at time delays relative to photoexcitation. Here a Fabry-Perot etalon was used instead of a grating filter to generate the Raman pump resulting in an exponential temporal profile instead of a Gaussian profile.

8. TIPS-Pentacene Experiments

To verify that the splitting features seen in our pentacene FSRS data do not arise from any sort of experimental artifact, we performed similar measurements on a 6,13-

Bis(triisopropylsilylethynyl)pentacene (TIPS-pentacene) sample. This sample consisted of 5 wt% TIPS-pentacene dissolved in toluene and spun-coat on a glass substrate. We observe prominent ground state features, but the transient spectra are very different from spectra obtained from pentacene crystals. The lack of any splitting features indicates that a charge-transfer intermediate is either not present or not observable by FSRS in TIPS-pentacene. Additionally, the results of these measurements confirm that the features seen in pentacene are not an artifact of the experiment or experimental setup.

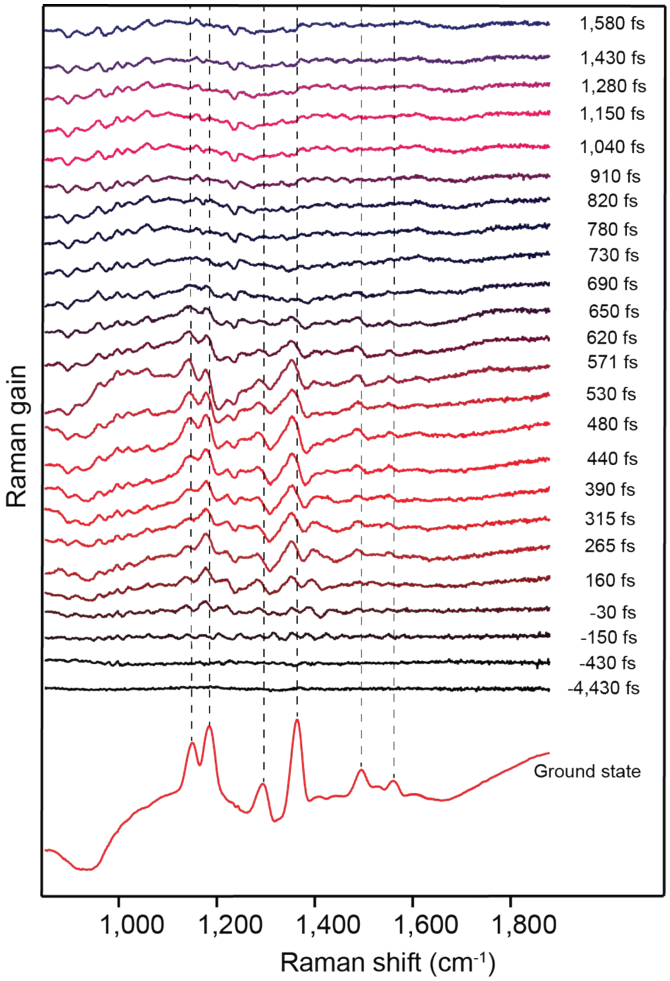

Figure S11. Femtosecond stimulated Raman spectra of TIPS-pentacene. The absence of any splitting features in the transient spectra indicates that the charge-transfer intermediate observed in pentacene is not observed in TIPS-pentacene.

9. DFT/TD-DFT Calculations

As described in the main text, DFT and TD-DFT calculations were performed for the neutral, anion and cation states of pentacene. Figure S12 shows the calculated Raman spectra, optimized geometry coordinates for these states are listed in tables S2 – S5, and converged energy values are listed in table S6.

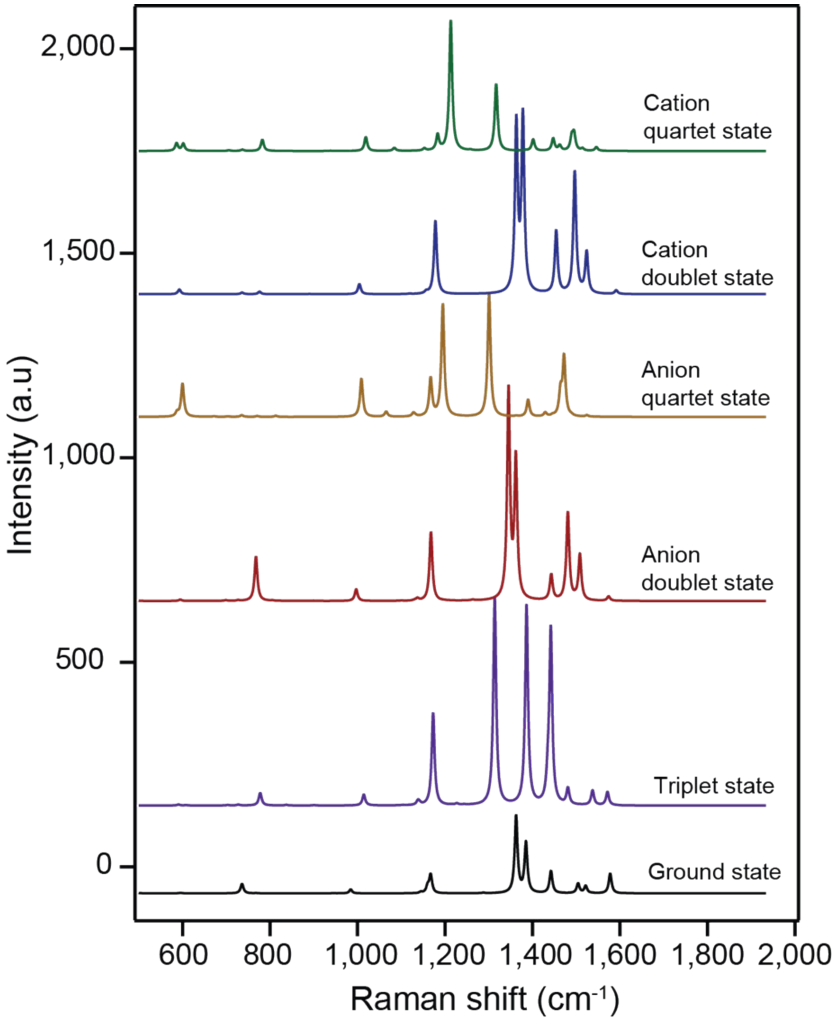

Figure S12. Calculated Raman spectra for the ground and first excited states of neutral, cationic and anionic pentacene.

Table S2. Optimized geometry for neutral pentacene ground state.

Atom Number	X	Y	Z
1	-2.464942	-1.406581	0.000000
2	-1.224816	-0.727749	0.000000
3	-1.224816	0.727749	0.000000
4	-2.464942	1.406581	0.000000
5	0.000000	-1.406972	0.000000
6	0.000000	1.406972	0.000000
7	1.224816	0.727749	0.000000
8	1.224816	-0.727749	0.000000
9	2.464942	-1.406581	0.000000
10	2.465539	-2.492436	0.000000
11	2.464942	1.406581	0.000000
12	-2.465539	-2.492436	0.000000
13	-2.465539	2.492436	0.000000
14	2.465539	2.492436	0.000000
15	3.673710	-0.726921	0.000000
16	3.673710	0.726921	0.000000
17	6.110146	0.716026	0.000000
18	7.055820	1.245993	0.000000
19	6.110146	-0.716026	0.000000
20	7.055820	-1.245993	0.000000
21	-3.673710	-0.726921	0.000000
22	-3.673710	0.726921	0.000000
23	-6.110146	-0.716026	0.000000
24	-7.055820	-1.245993	0.000000
25	-6.110146	0.716026	0.000000
26	-7.055820	1.245993	0.000000
27	-4.936409	-1.408889	0.000000
28	-4.936419	-2.493912	0.000000
29	-4.936409	1.408889	0.000000
30	-4.936419	2.493912	0.000000
31	4.936409	-1.408889	0.000000
32	4.936419	-2.493912	0.000000
33	4.936409	1.408889	0.000000
34	4.936419	2.493912	0.000000
35	0.000000	2.492712	0.000000
36	0.000000	-2.492712	0.000000

Table S3. Optimized geometry for the S1 state of neutral pentacene.

Atom Number	X	Y	Z
1	0.000000	2.463013	1.401310

2	0.000000	1.236256	0.726815
3	0.000000	1.236256	-0.726815
4	0.000000	2.463013	-1.401310
5	0.000000	0.000000	1.401440
6	0.000000	0.000000	-1.401440
7	0.000000	-1.236256	-0.726815
8	0.000000	-1.236256	0.726815
9	0.000000	-2.463013	1.401310
10	0.000000	-2.464455	2.487151
11	0.000000	-2.463013	-1.401310
12	0.000000	2.464455	2.487151
13	0.000000	2.464455	-2.487151
14	0.000000	-2.464455	-2.487151
15	0.000000	-3.701967	0.720891
16	0.000000	-3.701967	-0.720891
17	0.000000	-6.139701	-0.703196
18	0.000000	-7.080246	-1.241952
19	0.000000	-6.139701	0.703196
20	0.000000	-7.080246	1.241952
21	0.000000	3.701967	0.720891
22	0.000000	3.701967	-0.720891
23	0.000000	6.139701	0.703196
24	0.000000	7.080246	1.241952
25	0.000000	6.139701	-0.703196
26	0.000000	7.080246	-1.241952
27	0.000000	4.941559	1.400409
28	0.000000	4.942482	2.485473
29	0.000000	4.941559	-1.400409
30	0.000000	4.942482	-2.485473
31	0.000000	-4.941559	1.400409
32	0.000000	-4.942482	2.485473
33	0.000000	-4.941559	-1.400409
34	0.000000	-4.942482	-2.485473
35	0.000000	0.000000	-2.487351
36	0.000000	0.000000	2.487351

Table S4. Optimized geometry for pentacene cation.

Atom Number	X	Y	Z
1	-2.454583	-1.407804	0.000000
2	-1.227316	-0.726819	0.000000
3	-1.227316	0.726819	0.000000
4	-2.454583	1.407804	0.000000
5	0.000000	-1.409187	0.000000
6	0.000000	1.409187	0.000000

7	1.227316	0.726819	0.000000
8	1.227316	-0.726819	0.000000
9	2.454583	-1.407804	0.000000
10	2.457122	-2.492940	0.000000
11	2.454583	1.407804	0.000000
12	-2.457122	-2.492940	0.000000
13	-2.457122	2.492940	0.000000
14	2.457122	2.492940	0.000000
15	3.677326	-0.722990	0.000000
16	3.677326	0.722990	0.000000
17	6.104842	0.708891	0.000000
18	7.048642	1.240731	0.000000
19	6.104842	-0.708891	0.000000
20	7.048642	-1.240731	0.000000
21	-3.677326	-0.722990	0.000000
22	-3.677326	0.722990	0.000000
23	-6.104842	-0.708891	0.000000
24	-7.048642	-1.240731	0.000000
25	-6.104842	0.708891	0.000000
26	-7.048642	1.240731	0.000000
27	-4.922242	-1.408760	0.000000
28	-4.925642	-2.492816	0.000000
29	-4.922242	1.408760	0.000000
30	-4.925642	2.492816	0.000000
31	4.922242	-1.408760	0.000000
32	4.925642	-2.492816	0.000000
33	4.922242	1.408760	0.000000
34	4.925642	2.492816	0.000000
35	0.000000	2.494439	0.000000
36	0.000000	-2.494439	0.000000

Table S5. Optimized geometry for pentacene anion.

Atom Number	X	Y	Z
1	-2.473855	-1.401490	0.000000
2	-1.236036	-0.730794	0.000000
3	-1.236036	0.730794	0.000000
4	-2.473855	1.401490	0.000000
5	0.000000	-1.403561	0.000000
6	0.000000	1.403561	0.000000
7	1.236036	0.730794	0.000000
8	1.236036	-0.730794	0.000000
9	2.473855	-1.401490	0.000000
10	2.475531	-2.488956	0.000000
11	2.473855	1.401490	0.000000

12	-2.475531	-2.488956	0.000000
13	-2.475531	2.488956	0.000000
14	2.475531	2.488956	0.000000
15	3.702875	-0.724654	0.000000
16	3.702875	0.724654	0.000000
17	6.150375	0.708827	0.000000
18	7.092139	1.248757	0.000000
19	6.150375	-0.708827	0.000000
20	7.092139	-1.248757	0.000000
21	-3.702875	-0.724654	0.000000
22	-3.702875	0.724654	0.000000
23	-6.150375	-0.708827	0.000000
24	-7.092139	-1.248757	0.000000
25	-6.150375	0.708827	0.000000
26	-7.092139	1.248757	0.000000
27	-4.957399	-1.398956	0.000000
28	-4.957229	-2.485779	0.000000
29	-4.957399	1.398956	0.000000
30	-4.957229	2.485779	0.000000
31	4.957399	-1.398956	0.000000
32	4.957229	-2.485779	0.000000
33	4.957399	1.398956	0.000000
34	4.957229	2.485779	0.000000
35	0.000000	2.490802	0.000000
36	0.000000	-2.490802	0.000000

Table S6. Calculated energies for pentacene states.

State	Energy (Hartees)
S_0 (Ground State)	☐-846.99695812
S1 (Excited State)	-846.93257899
D_1 (Cationic State)	-847.05353066
D_1 (Anionic State)	☐-846.76970467

10. Excitation Wavelength Dependence

Here we probe the dependence of excited state dynamics with varying excitation wavelengths. In addition to the 570 nm excitation used in the main text, Figure S14 shows excited state dynamics comparison of three time points at within a 30 fs range -200 fs, -20 fs, and +225 fs for pentacene pumped at 600 nm, 570 nm, and 532 nm. Here slightly different time points were probed in the experiments at three different wavelengths, thus time points were selected for each wavelength such to represent a comparative time point range. The exact time points for all three wavelengths are as follows 600 nm: -200 fs, -30 fs, 230 fs; 532 nm: -240 fs, -40 fs, 210 fs; 570 nm: -255 fs, 1 fs, 240 fs.

Here the same peak splitting features are seen on the same timescale as for the 570 nm excitation, as seen in the transient absorption and Raman traces in Figure S15 (time points scaled to 570 nm transient absorption trace in all cases for clarity). Complete data sets (all time points) for pentacene pumped at 532 nm and 600 nm are shown in Figures S16 and S17, respectively. These data therefore suggest that the charge-transfer intermediate dynamics are seen regardless of excitation wavelength examined. Thus the peak-splitting phenomena is likely not due to the addition of extra energy into the system that could promote the singlet to higher lying vibrational levels upon excitation.

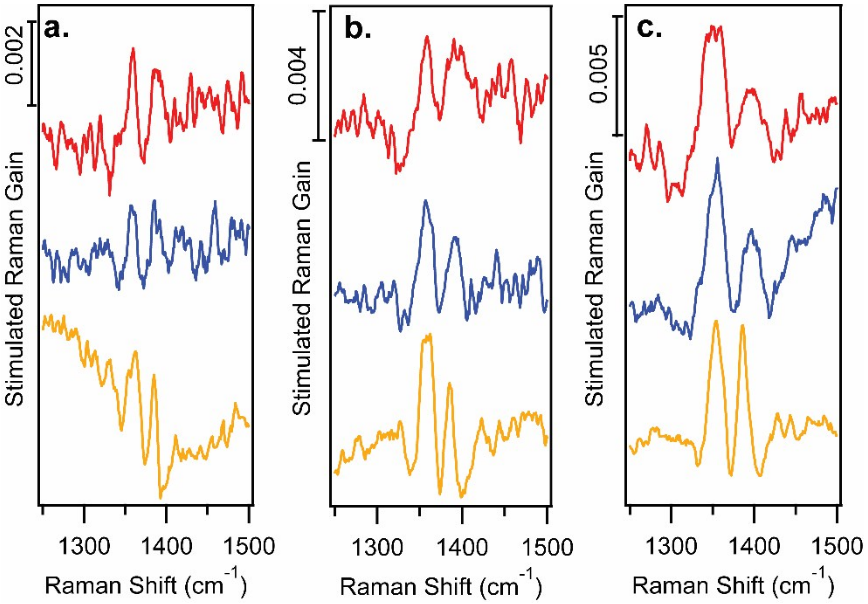

Figure S13. Excited state pentacene dynamics at (a) -200 fs (b) -20 fs (c) +225 fs. Red pumped at 600 nm, blue pumped at 532 nm, and yellow pumped at 570 nm.

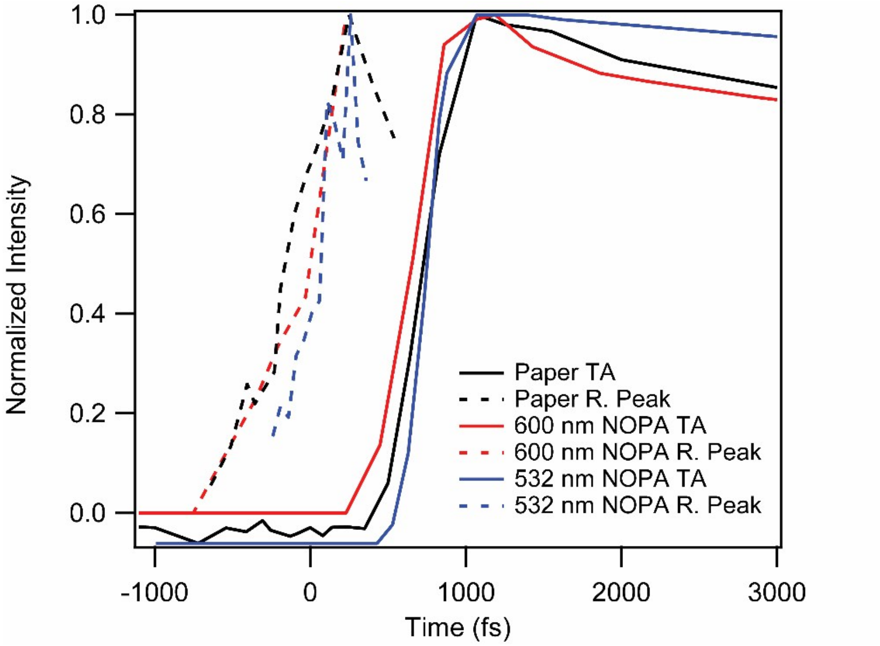

Figure S14. Pentacene 1374 cm^{-1} blue shifted exited state peak dynamics and transient absorption at 600 nm, 570 nm, and 532 nm actinic pump excitation.

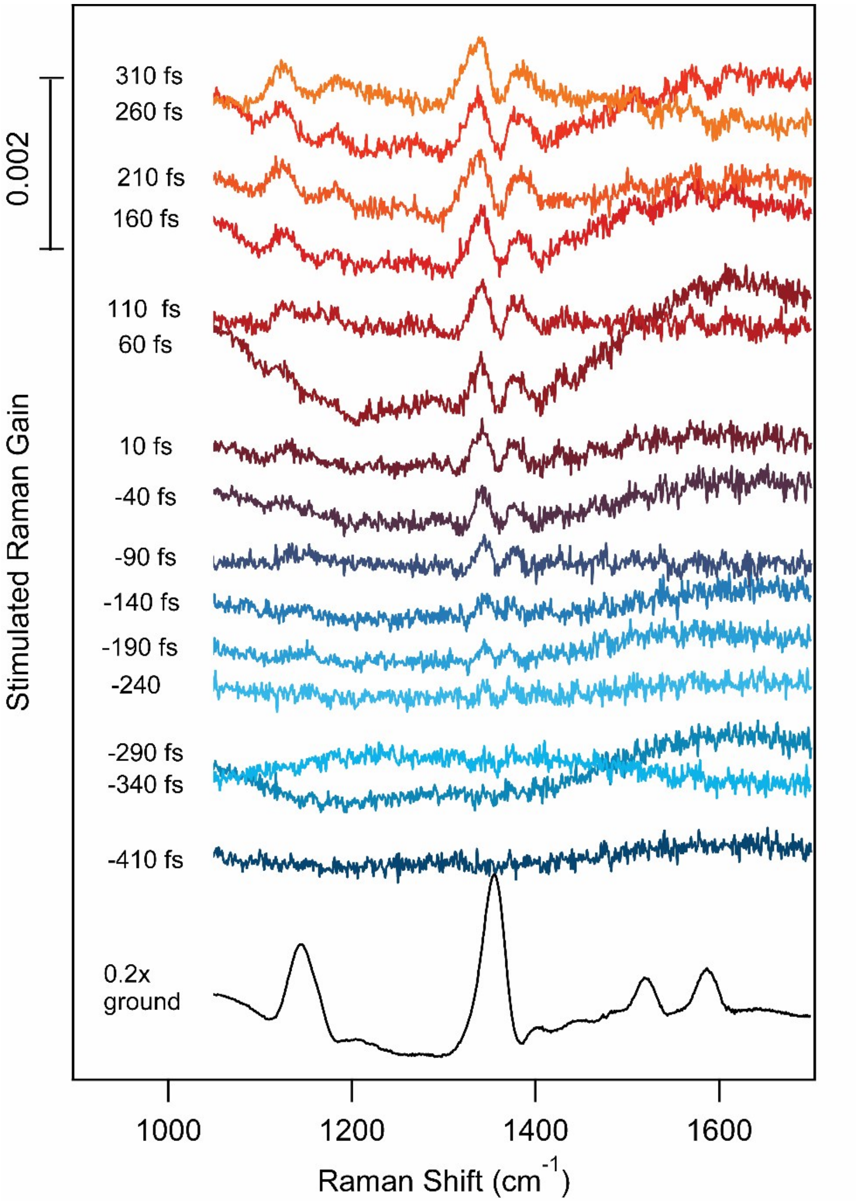

Figure S15. Differential stimulated Raman spectra pumped at 532 nm.

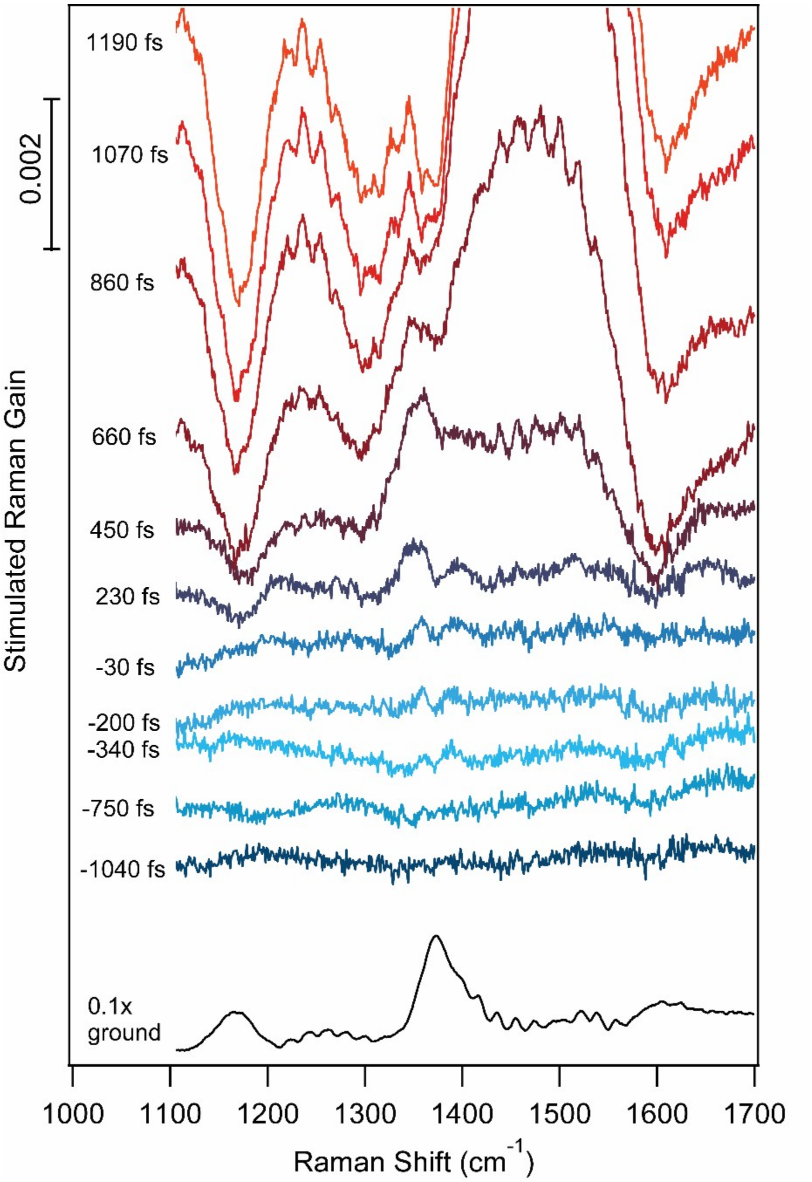

Figure S16. Differential stimulated Raman spectra pumped at 600 nm.

References

1. Musser, A. J., Liebel, M., Schnedermann, C., Wende, T., Kehoe, T. B., Rao, A., Kukura, P. Evidence for conical intersection dynamics mediating ultrafast singlet exciton fission. *Nat. Phys.* **11,** 352-357 (2015).

2. Bakulin, A. A., Morgan, S. E., Kehoe, T. B., Wilson, M. W. B., Chin, A. W., Zigmantas, D., Egorova, D., Rao, A. Real-time observation of multiexcitonic states in ultrafast singlet fission using coherent 2D electronic spectroscopy. *Nat. Chem.* **8,** 16-23 (2015).

3. Sharifzadeh, S., Darancet, P., Kronik, L., Neaton, J. B. Low-energy charge-transfer excitons in organic solids from first-principles: The case of pentacene. *J. Phys. Chem. Lett.* **4,** 2197-2201 (2013).

4. Liebel, M., Schnedermann, C., Wende, T., Kukura, P. Principles and applications of broadband impulsive vibrational spectroscopy. *J. Phys. Chem. A.* **119**, 9506-9517 (2015).

5. Silva, W. R., Keller, E. L., Frontiera, R. R. Determination of resonance Raman cross-sections for use in biological SERS sensing with femtosecond stimulated Raman spectroscopy. *Anal. Chem.* **86,** 7782-7787 (2014).